Hindawi
Geofluids
Volume 2020, Article ID 8830862, 9 pages
https://doi.org/10.1155/2020/8830862

Research Article

Coupled Hydraulic-Thermal Modelling and Related Numerical Analysis on Rock Fractures

Yongjian Pan,[1] Huajun Wang,[1] and Qiang Liu[2,3]

[1]*Zhejiang Engineering Survey and Design Institute Group Co. Ltd., Ningbo, 315010 Zhejiang Province, China*
[2]*Work Safety Key Lab on Prevention and Control of Gas and Roof Disasters for Southern Coal Mines, Hunan University of Science and Technology, Xiangtan, 411201 Hunan Province, China*
[3]*School of Resource Environment and Safety Engineering, Hunan University of Science and Technology, Xiangtan, 411201 Hunan Province, China*

Correspondence should be addressed to Qiang Liu; pexliuqiang@163.com

Received 23 August 2020; Revised 30 September 2020; Accepted 9 November 2020; Published 23 November 2020

Academic Editor: Yixian Wang

Hydraulic-thermal coupling is a key problem in rock mass engineering, especially in the disposal of nuclear wastes in deep rock mass. To accurately describe the coupling action of rock mass when under the interaction of hydraulic stress and thermal, the hydraulic-thermal coupling solving methods were proposed in this paper; in addition, the corresponding hydraulic-thermal coupling program FRHT3D was complied. Consequently, the numerical simulation was performed, it can be concluded that the flow speed is faster when the coupling effect is considered at the unstable seepage stage, and the seepage coupling solution is larger than that of uncoupling. Furthermore, when the coupling effects are considered, the permeable water head solution is much larger than that of the uncoupling solution at the unstable seepage stage. The proposed hydraulic-thermal coupling solving methods and programs can be applied to rock mass engineering practice.

1. Introduction

Hydraulic-thermal coupling is one of the most important subsystems of the thermal-hydraulic-mechanical (THM) system; it is a new research area with wide application. The thermal-hydraulic coupling process and mechanism of rock mass are conducive to petroleum excavation, natural gas excavation, underground water excavation, geothermal resource development, and disposal of nuclear wastes in deep rock mass. Besides, there exist problems in large water conservation and hydropower project in the river and gorge; the related study is critically important for the stability of water conservation and hydropower project. At present, the study on the hydraulic-thermal coupling mechanism of rock mass with fissures is mainly based on the continuum and equivalent continuum seepage theory. With regard to the study of THM coupling, how to simulate the process of hydraulic-thermal coupling of rock mass with fissures with noncontinuum theory has become a hot topic.

McDermott et al. [1] presented such an approach for the simulation of fluid flow through a fracture validated against experimental data and cross-comparison with results of other modelling teams within the DECOVALEX 2015 project by replacing the mechanical behavior and chemical transport process within physical models, and some results of thermal-hydraulic-mechanical-chemical conditions for fracture rock were attained. Cacace and Jacquey [2] developed theory and numerical implementation describing groundwater flow and the transport of heat and solute mass in fully saturated rocks with elastoplastic mechanical feedbacks; in the model, fractures were considered being of lower dimension than the hosting deformable porous rock. Ogata et al. [3] developed a multiphysics numerical model to predict the fluid flow and mass transport behavior of rock fractures under coupled thermal-hydraulic-mechanical-chemical conditions. Particularly, the model was employed for the purpose of describing the evolution of permeability and reactive transport behavior within rock fractures by

taking into account the geochemical processes of the free-face dissolution and the pressure dissolution. Liu et al. [4] proposed a coupled thermal-hydraulic-chemical model to study the influence of rock heterogeneity and the coupling effect of temperature, groundwater, and hydrochemistry on rock damage, and an actual deep coal mine model was established to predict water inrush. Furthermore, Shao et al. [5, 6], Olsson and Barton [7], Xie et al. [8], Zhang and Nemcik [9], Tsang and Witherspoon [10], and many other scholars [11–24] studied the rheological fracture behavior of rock cracks subjected and the coupling effect of rock, which promoted the development of mechanical characteristics of rocks under complicated conditions.

Though some numerical simulation software, such as FLAC and 3DEC, can simulate the THM coupling, this coupling is one-way coupling, which only considered the influence of the thermal field to the seepage field. Meanwhile, the heat transform coefficient, heat conductivity coefficient, and width of cracks are constant; however, many researches proved that the heat transform coefficient h is related to the width of fissures.

In this paper, the fluid mechanics and boundary layer theory of heat conductivity theory were applied to the study of water-rock heat transform, and the heat transform between single fissure interface and water fluid was analyzed, its hydraulic-thermal model was established, and the effect of hydraulic-thermal coupling was systematically studied.

2. Hydrothermal Theory and Its Implementation

2.1. Basic Assumptions. The seepage field and thermal field of discrete fissure net interact. On the one hand, the variation of fissure seepage of rock mass could influence the transmitting and exchange of water fluid and fissure interface, which further changes the distribution of the thermal field; on the other hand, the variation of the thermal field could change the fluid viscosity and density, influencing the distribution of the crack seepage field. For convenience of establishing the noncontinuum hydraulic-thermal coupling model of rock mass, some basic assumptions are as follows.

(1) Rock mass consists of impermeable rock and rock fissures; the fissure is the channel of rock mass seepage

(2) The fluid in fissure seepage cannot be compressed, and it obeys Darcy's law and cubic law

(3) The heat in rock is transmitted by heat conduction; the heat of water can be transmitted by heat conduction and thermal convection, which occurs on the interface of rock and water

2.2. Hydraulic-Thermal Coupling Equation. Hydraulic-thermal analysis systems of noncontinuum rock mass include thermal field analysis of rock-fissure water, seepage field of fissures, and hydraulic-thermal coupling parameter transmitting analysis.

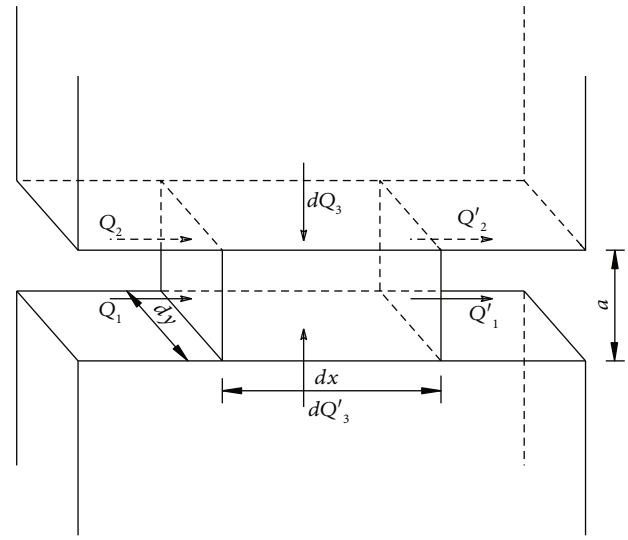

Figure 1: Heat equilibrium of fluid in fissure for a calculation unit.

2.2.1. Thermal Field Analysis of Water in Fissures. Heat transmission of thermal field analysis of rock seepage can be summarized: fluid-fluid heat transmission, thermal convection of fluid-fluid, and thermal convection of rock-fluid, which is displayed in Figure 1.

As regard to thermal convection of fluid-fluid, the heat flux variation of unit thickness on the $x-y$ plane can be denoted as

$$\begin{aligned} dQ_{\text{conv}} &= dQ_1 = Q_1 - Q_1' \\ &= -\int_{(D)} \rho_w C_{vw} \left(v_x \frac{\partial T_w}{\partial x} + v_y \frac{\partial T_w}{\partial y} \right) dxdy. \end{aligned} \tag{1}$$

The heat flux variation is

$$\begin{aligned} dQ_{\text{cond}} &= dQ_2 = Q_2 - Q_2' \\ &= -\int_{(D)} \lambda_w \left[\frac{\partial}{\partial x} \left(\frac{\partial T_w}{\partial x} \right) + \frac{\partial}{\partial y} \left(\frac{\partial T_w}{\partial y} \right) \right] dxdy. \end{aligned} \tag{2}$$

The heat flux variation of rock-fluid thermal convection can be expressed as

$$dQ_3^a = h(T_{rb} - T_w)dx, \tag{3}$$

$$dQ_3^b = h\left(T'_{rb} - T_w\right)dx, \tag{4}$$

$$dQ_3 = dQ_3^a + dQ_3^b, \tag{5}$$

where ρ_w is the fluid density; C_{vw} is the fluid heat capacity; v_x, v_y is the flow velocity in the x, y direction; T_w is the temperature of fluid; λ_w is the fluid heat conductivity; h is the fluid thermal coefficient; and T_{rb}, T'_{rb} is the boundary temperature near fissure.

Heat conduction coefficient h is related to characteristics of fissure interface, fluid speed, viscosity, and boundary condition. Midoux reckoned that the heat conduction coefficient h can be expressed as follows:

$$h = \frac{\lambda_w N_{u_L}}{2a} = \frac{3.549\lambda_w}{2a}\left[\frac{\rho_w v_i C_{pw}(2a)^2}{\lambda_w L}\right]^{1/3} = \frac{3.549\lambda_w}{2a}\left[G_{Z_L}\right]^{1/3}, \tag{6}$$

where v_i is the fluid speed along the fissure direction; a is the width of crack; L is the characteristic length related to the dimension of the problem; N_{u_L} is the Nusselt coefficient; and G_{Z_L} is the Graetz coefficient.

Figure 1 illustrates the heat entry and exit diagram of fluid in a fissure. The heat equilibrium of a fluid unit can be expressed as

$$\rho_w c_{vw}\frac{dT_w}{dt} = dQ_1 + dQ_2 + dQ_3, \tag{7}$$

$$c_{vw}\rho_w\frac{\partial T_w}{\partial t} = \lambda_w\nabla^2 T - c_{pw}\cdot\rho_w\cdot\nabla(v_i\cdot T_w) + h(T_{rb} - T_w). \tag{8}$$

It obeys Darcy's law in fissure fluid, which can be expressed as

$$v_i = q_i = k_f\nabla p, \quad i = x, y, z, \tag{9}$$

$$k_f = \frac{\beta g a^2}{12\nu}, \tag{10}$$

where v_i is the fluid speed, q_i is the flow rate, k_f is the permeable coefficient, β is the fracture connectivity, and ν is the flow viscosity of fluid.

Adopting the C_0 interpolation function of the Galerkin method, functional equations can be dispersed; then, the finite element discrete equation of the thermal field was attained:

$$\{K_w\Delta t + C_w\}T_{w(t+\Delta t)} = K_w T_{w(t)} + P_w\Delta t, \tag{11}$$

where C_w is the thermal capacity matrix, K_w is the heat conduction matrix, P_w is the temperature load matrix, T_w is the junction temperature matrix, and Δt is the time step, where the matrix element in Equation (11) can be expressed as follows:

$$K^e_{wij} = \int_{\Omega^e}\lambda_w\left(\frac{\partial N_i}{\partial x}\frac{\partial N_j}{\partial x} + \frac{\partial N_i}{\partial y}\frac{\partial N_j}{\partial y} + \frac{\partial N_i}{\partial z}\frac{\partial N_j}{\partial z}\right)d\Omega + \int_{\Omega^r} C_{pw}\rho_w k_f N_j\left(\frac{\partial N_i}{\partial x}\frac{\partial H}{\partial x} + \frac{\partial N_i}{\partial y}\frac{\partial H}{\partial y} + \frac{\partial N_i}{\partial z}\frac{\partial H}{\partial z}\right), \tag{12}$$

$$C^e_{wij} = \int_{\Omega^e} c_{vw}\cdot\rho_w\cdot N_i\cdot N_j\cdot d\Omega, \tag{13}$$

$$P^e_{wi} = \int_{\Omega^e} N_i\cdot h(T_{rb} - T_w(t))d\Omega, \tag{14}$$

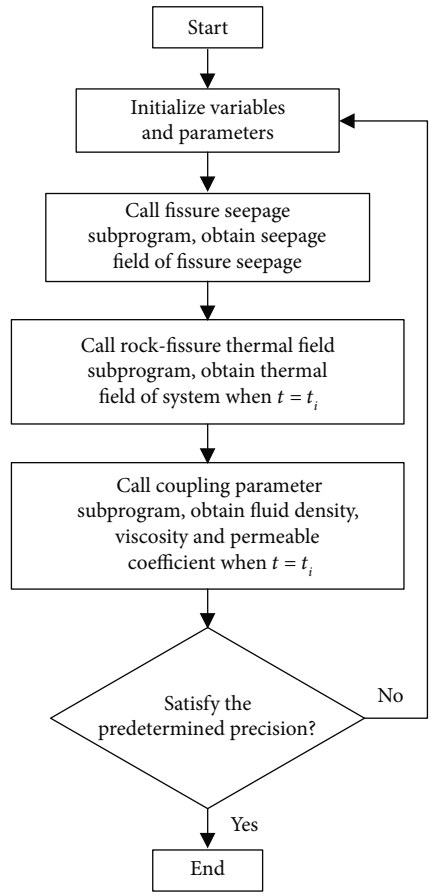

Figure 2: Procedure of fluid-thermal coupling.

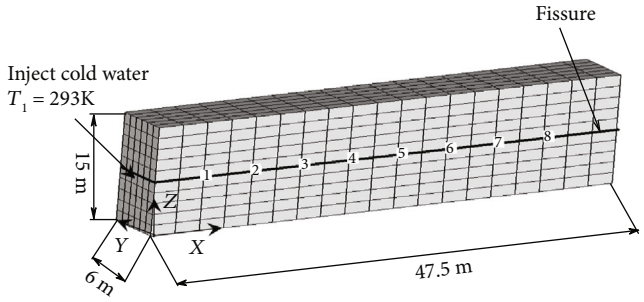

Figure 3: Numerical simulation model.

where N_i, N_j are the interpolation functions and H is the water head.

2.2.2. Thermal Field Analysis. The heat in rock is transmitted by the way of heat conduction; the heat theory can be expressed as follows:

$$\rho_r c_{pr}\frac{\partial T_r}{\partial t} = \lambda_r\nabla^2 T_r + W, \tag{15}$$

Table 1: Basic parameters of the fluid-thermal coupling numerical model.

Medium	Density (kg/m^3)	Thermal conductivity (W/m/K)	Heat absorption capacity coefficient (J/kg/K)	Initial permeable coefficient (m/s)	Hydraulic opening (μm)	Specific water storage coefficient (m^{-1})
Rock	2.7×10^3	2.58	1.0×10^3			
Fluid	1000	0.6	4.0×10^3	2.23×10^{-4}	50	0.007

where ρ_r is the rock density, c_{pr} is the specific heat at constant pressure of rock, T_r is the temperature of rock, λ_r is the thermal conductivity of rock, and W is the heat source sink.

C_0 interpolation function using the Galerkin method was adopted, the functional equation was dispersed, and the thermal field distribution was attained:

$$\{K\Delta t + C\}T_{r(t+\Delta t)} = KT_{r(t)} + P\Delta t, \tag{16}$$

where C is the heat capacity matrix, K is the heat conduction matrix of rock, P is the temperature load matrix of rock, T_r is the junction load temperature matrix of rock, and Δt is the time step. The element matrix in Equation (6) was depicted as follows:

$$K_{ij}^e = \int_{\Omega^e} \lambda_r \left(\frac{\partial N_i}{\partial x}\frac{\partial N_j}{\partial x} + \frac{\partial N_i}{\partial y}\frac{\partial N_j}{\partial y} + \frac{\partial N_i}{\partial z}\frac{\partial N_j}{\partial z} \right) d\Omega, \tag{17}$$

$$C_{ij}^e = \int_{\Omega^e} c_{pr}\rho_r N_i N_j d\Omega, \tag{18}$$

$$P_i^e = \int_{\Omega^e} W \cdot N_i \cdot d\Omega + \int_{\Gamma_2^e} q \cdot N_i \cdot d\Gamma + \int_{\Gamma_3^e} h \cdot T_{ra} \cdot N_i \cdot d\Gamma. \tag{19}$$

2.2.3. Seepage Field Analysis in Fissure. Based on the law of conservation of mass, the conservation of mass of any unit controlled by fissure can be determined by the following equation:

$$\frac{\partial}{\partial x'}\left(k_f \frac{\partial h}{\partial x'}\right) + \frac{\partial}{\partial y'}\left(k_f \frac{\partial h}{\partial y'}\right) = s\frac{\partial h}{\partial t}, \tag{20}$$

where h is the water head, s is the specific water storage coefficient, and x' and y' are the local coordinates.

C_0 interpolation function using the Galerkin method was adopted, the functional equation is dispersed, and the finite element discrete equation of the seep field is attained:

$$\{T\Delta t + S\}P_{t+\Delta t} = SP_t + H\Delta t, \tag{21}$$

Table 2: Calculation parameters of the numerical model without considering hydraulic-thermal coupling.

Water temperature (K)	Density (kg/m^3)	Viscosity (m^2/s)	Permeable coefficient (m/s)	Heat transform coefficient (W/m^2/K)
293	1.0×10^3	0.885×10^{-6}	0.95×10^{-4}	2.25×10^4

where T, S, H is the transmitting matrix, storage matrix, and column vector, respectively. The corresponding unit matrix can be depicted as follows:

$$T_{ij}^e = a\int_{\Omega^e} k_f \left(\frac{\partial N_i}{\partial x'}\frac{\partial N_j}{\partial x'} + \frac{\partial N_i}{\partial y'}\frac{\partial N_j}{\partial y'} \right) d\Omega, \tag{22}$$

$$S_{ij}^e = s\int_{\Omega^e} N_i N_j d\Omega, \tag{23}$$

$$H_i^e = \int_{\Gamma_2^e} g \cdot N_i \cdot d\Gamma. \tag{24}$$

2.2.4. Fluid-Thermal Coupling Coefficient Transmitting Analysis. With respect to the fluid-thermal coupling analysis of noncontinuum, the main coupling parameters, such as fluid density ρ_w, viscosity v, seepage coefficient k_f, and heat conductivity h could be determined:

$$\rho_w = -0.0035T^2 - 0.0817T + 1001, \tag{25}$$

$$v = 0.1853T^{-0.8962}, \tag{26}$$

$$k_f = \frac{\beta g b^2}{12 \times 0.1853T^{-0.8962}}, \tag{27}$$

$$h = \frac{3.549\lambda_w}{2a}\left[\frac{\rho_w v_i c_{pw}(2a)^2}{\lambda_w L}\right]^{1/3}. \tag{28}$$

2.3. Program for Fluid-Thermal Coupling of Noncontinuum Rock. The fluid-thermal mathematical model of

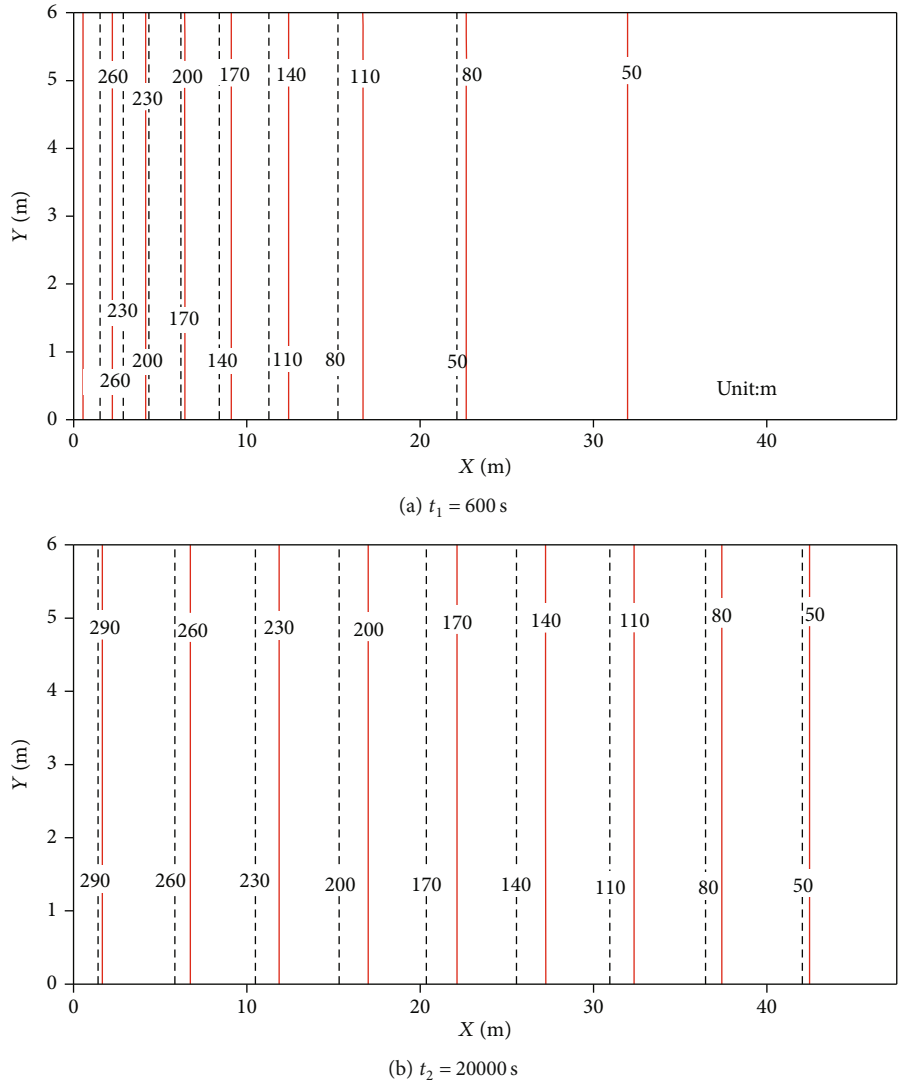

Figure 4: Isometric line of the seepage field in the fissure interface.

noncontinuum rock is a nonlinear three-dimensional parabola equation, these equations consist of many coupling parameters and variables, they are hard to be solved even for a one-dimensional problem, and we complied the numerical simulation program FRHT3D of fluid-coupling of noncontinuum rock mass. A planar four-node unit was used for the planar fissure; eight nodes in space are used for the rock. The solving systems contain two subsystems: fissure seepage and rock system and thermal seepage field system. The main solving procedure is illustrated in Figure 2.

3. Fluid-Thermal Coupling Effect of Noncontinuum Rock Mass

3.1. Numerical Simulation Model. To study the hydrothermal coupling effect of noncontinuum rocks, the calculation example is established in Figure 3. The size of the numerical simulation model is $x \times y \times z = 47.5\,\text{m} \times 6\,\text{m} \times 15\,\text{m}$, a total of 1680 grid points and 1254 coupling zones are included in the numerical simulation model, the fissure is placed $z = 3\,\text{m}$, it is parallel with the bottom of the numerical model, and the hydraulic opening of fissure is $a = 50\,\mu\text{m}$.

The initial and boundary condition of seepage is that the fissure is kept with the state of saturation, its initial water head is $h_0 = 20\,\text{m}$, the water head of the left numerical model is $h_1 = 300\,\text{m}$, it is kept at this state during the numerical simulation, and the right water head is $h_2 = 20\,\text{m}$.

The initial temperature condition is $T_0 = 293\,\text{K}$, the left side of the numerical model is injected with cold water with temperature of $T_1 = 293\,\text{K}$, and the boundary condition of the rock interface and water interface is as follows:

$$-\lambda_w \left.\frac{\partial T_w}{\partial n}\right|_{\Gamma(x,y)} = h(T_{rb} - T_w). \tag{29}$$

The basic mechanical parameters of the hydraulic-thermal coupling model are listed in Table 1. During the numerical simulation, the water head and temperature 1-8# were recorded at different time points.

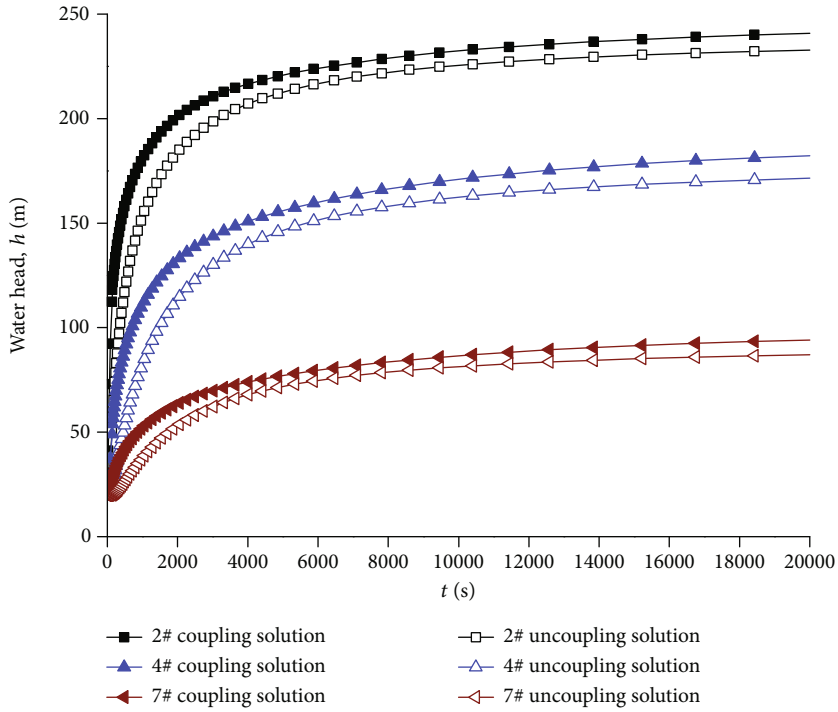

Figure 5: Water head evolution at the nodes 2#, 4#, and 7# in the fissure interface.

To study the hydraulic-thermal coupling effect of noncontinuum rock mass, the coupling and uncoupling numerical simulation would be analyzed; the uncoupling parameters are listed in Table 2.

3.2. Hydraulic-Thermal Coupling Effect

3.2.1. Coupling Effect of Thermal Field to Seepage Field. The coupling effect of the thermal field to the seepage field is mainly due to the fact that fluid density, viscosity, and permeable coefficient are the function of fluid temperature; the variation of fluid temperature leads to the variation of seepage control equations, which influence the distribution of the fluid field. Figure 4 gives the seepage field distribution when $t_1 = 600$ s and $t_2 = 20000$ s; the solid line represents the coupling calculation results, while the dotted line represents the uncoupling numerical simulation results. From the analysis of Figure 4, it could be concluded that there exists a big difference for numerical simulation results when the coupling effects are considered or not. By comparison of Figures 4(a) and 4(b), the water head increased faster when the coupling effects are considered; the permeable water head solution is much larger than that of the uncoupling solution at the unstable seepage stage. With the development of seepage, the difference of coupling solution and uncoupling solution becomes smaller; in particular, the calculation results are close when $t_2 = 20000$ s.

3.3. Coupling Effect of Seepage Field to Thermal Field. Figure 5 illustrates the seepage water head evolution difference of nodes 2#, 4#, and 7# when the coupling effect was considered or not; it could be concluded that the coupling results and uncoupling results show the same increased trend; at the initial seepage stage, the increased speed of coupling solution is faster than the later, the time for seepage tending to a constant value. When the coupling effect is not considered, the water temperature is kept at 293 K; when the coupling effect is considered, the temperature of fissure water changed with the development of seepage; during the whole coupling numerical simulation, the temperature of water flow is higher than 293 K when the coupling effect is considered. The higher the temperature is, the larger the viscosity is, which results in the increase of the permeable coefficient. Therefore, the flow speed is faster when the coupling effect is considered at the unstable seepage stage, and the seepage coupling solution is larger than that of uncoupling.

The temperature of injected water ($T_1 = 293$ K) is lower than that of rock, the heat of rock is transmitted to water, and the flow water reduces the heat, which further changes the thermal field distribution of rock. The influence of the seepage field to the thermal field is mainly caused by two aspects: (1) thermal forced convection of the seepage flow and (2) thermal convection of seepage flow and rock surface. With the increase of water flow speed, two kinds of thermal convection accelerate both. Due to the increase in water flow speed, the heat transfer coefficient h increases; the influence of the seepage field coupling effect could be more apparent. At the unstable seepage stage, water flow is larger when the hydraulic-thermal coupling effect is considered; the cooling effect of water to rock is more significant when the coupling effect is considered, which can be observed in Figure 6; there exists an obvious difference in the thermal field when coupling effect is considered or not for $t_1 = 600$ s and $t_2 = 20000$ s; the thermal field is lower when the coupling effect is considered. Meanwhile, the temperature decreased

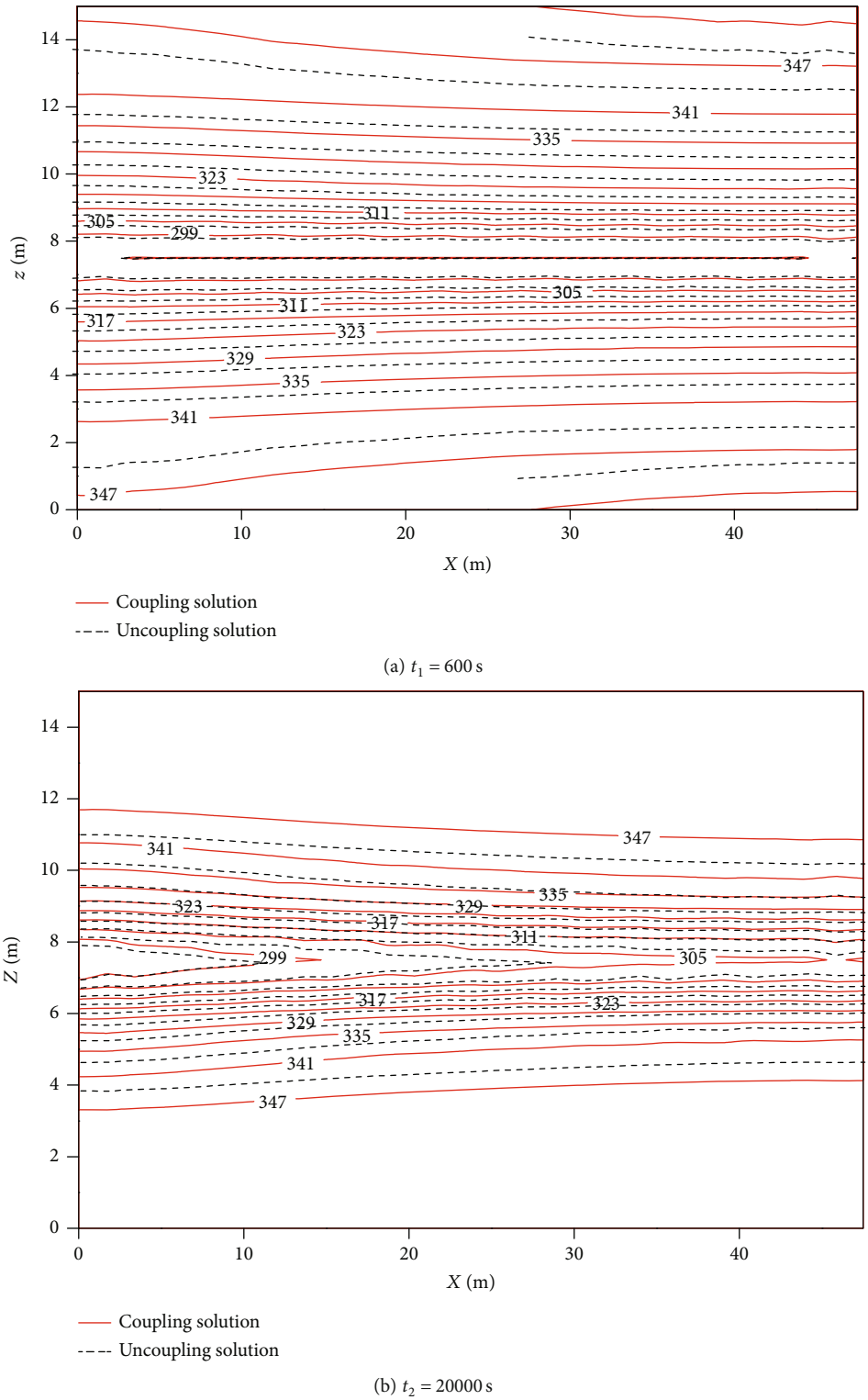

FIGURE 6: Comparison of the thermal field in x-z plane when the coupling effect is considered or not at different times.

remarkably near the rock, and the temperature increases towards the rock internal.

3.3.1. Coupling Effect of Calculation Parameters. The coupling parameters of hydraulic-thermal coupling of nonconti-nuum rock mass and the main coupling parameters include fluid density ρ_w, viscosity v, permeable coefficients k_{fi}, and heat conductivity h.

As regards heat conductivity h within a short time at the initial stage of seepage, due to the increase of hydraulic

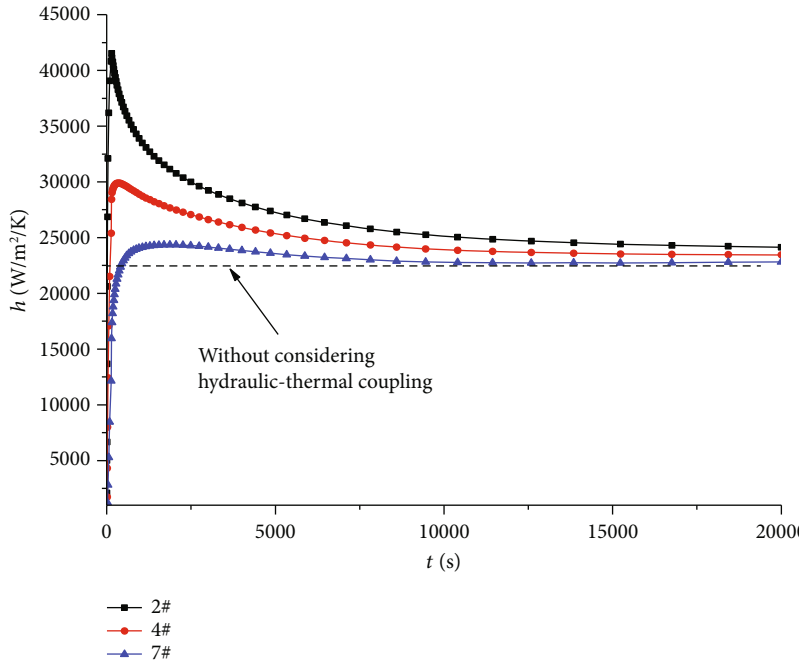

Figure 7: Heat conductivity h evolution of 2#, 4#, and 7# under the condition of hydraulic-thermal coupling.

gradient of every node, the flow speed increases; then, the heat conductivity increases subsequently; with the decrease of permeable coefficient, the flow speed slows down and the heat conductivity decreases. At the unstable stage, 2# is quite close to the location of water injection; the hydraulic gradient of 2# is larger than that of 4# and 7#. Due to the fact that flow speed of 2# is higher than 4# and 7#, the heat conductivity h of 2# is larger than that of 4# and 7#. With the development of seepage, the seepage tends to be stable, the rate of flow for the nodes tends to be a constant value, the heat conductivity all tends to be 2.35×10^4 W/m^2/K, and the heat conductivity h of 2#, 4#, and 7# under the action of hydraulic-thermal coupling could be shown in Figure 7.

4. Conclusions

The hydraulic-thermal coupling phenomenon is widely existing in rock mass engineering,to better predict the rock mass engineering stability, the hydraulic-thermal coupling solving methods were proposed, based on the methods, the corresponding program was complied; finally, the numerical simulation of hydraulic-thermal coupling was performed. The results of this paper can be summarized as below.

(1) The influence between the seepage field and the thermal field was analyzed; meanwhile, the corresponding theory was applied to implement the influence between the seepage field and the thermal field. Meanwhile, the fortran program FRHT3 was complied to simulate the hydraulic-thermal coupling

(2) Through the numerical simulation, it can be concluded that the flow speed is faster when the coupling effect is considered at the unstable seepage stage, and the seepage coupling solution is larger than that of uncoupling. Furthermore, when the coupling effects are considered, the permeable water head solution is much larger than that of the uncoupling solution at the unstable seepage stage

Data Availability

All data and models generated or used during the study appear in the submitted article.

Conflicts of Interest

The authors declare that they have no conflicts of interest.

Acknowledgments

This research is supported by the National Natural Science Foundation of China (Nos. 51774131 and 51274097). The authors are thankful for all of the support for this basic research.

References

[1] C. McDermott, A. Bond, A. F. Harris, N. Chittenden, and K. Thatcher, "Application of hybrid numerical and analytical solutions for the simulation of coupled thermal, hydraulic, mechanical and chemical process during fluid flow through a fractured rock," *Environmental Earth Sciences*, vol. 74, no. 12, pp. 7837–7854, 2015.

[2] M. Cacace and A. B. Jacquey, "Flexible parallel implicit modelling of coupled thermal-hydraulic-mechanical processes in fractured rocks," *Solid Earth*, vol. 8, no. 5, pp. 921–941, 2017.

[3] S. Ogata, H. Yasuhara, N. Kinoshita, D. S. Cheon, and K. Kishida, "Modeling of coupled thermal-hydraulic-mechanical-chemical processes for predicting the evolution in permeability and reactive transport behavior within single rock fractures," *International Journal of Rock Mechanics and Mining Sciences*, vol. 107, pp. 271–281, 2018.

[4] W. T. Liu, J. Y. Zhao, R. A. Nie, Y. F. Zeng, B. C. Xu, and X. Sun, "A full coupled thermal-hydraulic-chemical model for heterogeneity rock damage and its application in predicting water inrush," *Applied Sciences*, vol. 9, no. 11, p. 2195, 2019.

[5] J. F. Shao, Q. Z. Zhu, and K. Su, "Modeling of creep in rock materials in terms of material degradation," *Computers and Geotechnics*, vol. 30, no. 7, pp. 549–555, 2003.

[6] J. F. Shao, H. Zhou, and K. T. Chau, "Coupling between anisotropic damage and permeability variation in brittle rocks," *International Journal for Numerical and Analytical Methods in Geomechanics*, vol. 29, no. 12, pp. 1231–1247, 2010.

[7] R. Olsson and N. Barton, "An improved model for hydromechanical coupling during shearing of rock joints," *International Journal of Rock Mechanics and Mining Sciences*, vol. 38, no. 3, pp. 317–329, 2001.

[8] N. Xie, J. B. Yang, and J. F. Shao, "Study on the hydromechanical behavior of single fracture under normal stresses," *KSCE Journal of Civil Engineering*, vol. 18, no. 6, pp. 1641–1649, 2014.

[9] Z. Zhang and J. Nemcik, "Friction factor of water flow through rough rock fractures," *Rock Mechanics and Rock Engineering*, vol. 46, no. 5, pp. 1125–1134, 2013.

[10] Y. W. Tsang and P. A. Witherspoon, "Hydromechanical behavior of a deformable rock fracture subject to normal stress," *Journal of Geophysical Research: Solid Earth*, vol. 86, no. B10, pp. 9287–9298, 1981.

[11] J. Rutqvist and O. Stephansson, "The role of hydromechanical coupling in fractured rock engineering," *Hydrogeology Journal*, vol. 11, no. 1, pp. 7–40, 2003.

[12] M. Bart, J. F. Shao, D. Lydzba, and M. Haji-Sotoudeh, "Coupled hydromechanical modeling of rock fractures under normal stress," *Canadian Geotechnical Journal*, vol. 41, no. 4, pp. 686–697, 2004.

[13] X. Fan, K. H. Ki, H. P. Lai, Y. L. Xie, R. H. Cao, and J. Zheng, "Internal stress distribution and cracking around flaws and openings of rock block under uniaxial compression: a particle mechanics approach," *Computers and Geotechnics*, vol. 102, no. 10, pp. 28–38, 2018.

[14] P. F. Wang, C. Tian, R. H. Liu, and J. Wang, "Mathematical model for multivariate nonlinear prediction of SMD of X-type swirl pressure nozzles," *Process Safety and Environmental Protection*, vol. 125, pp. 228–237, 2019.

[15] P. F. Wang, Y. J. Li, R. H. Liu, and Y. J. Shi, "Effects of forced-to-exhaust ratio of air volume on dust control of wall-attached swirling ventilation for mechanized excavation face," *Tunnelling and Underground Space Technology*, vol. 90, pp. 194–207, 2019.

[16] L. Jing, "A review of techniques, advances and outstanding issues in numerical modelling for rock mechanics and rock engineering," *International Journal of Rock Mechanics and Mining Sciences*, vol. 40, no. 3, pp. 283–353, 2003.

[17] C. E. Manning and S. E. Ingebritsen, "Permeability of the continental crust: implications of geothermal data and metamorphic systems," *Reviews of Geophysics*, vol. 37, no. 1, pp. 127–150, 1999.

[18] L. Jing and J. A. Hudson, "Numerical methods in rock mechanics," *International Journal of Rock Mechanics and Mining Sciences*, vol. 39, no. 4, pp. 409–427, 2002.

[19] B. Li, Y. Jiang, T. Koyama, L. Jing, and Y. Tanabashi, "Experimental study of the hydro-mechanical behavior of rock joints using a parallel-plate model containing contact areas and artificial fractures," *International Journal of Rock Mechanics and Mining Sciences*, vol. 45, no. 3, pp. 362–375, 2008.

[20] A. Gens, M. Sanchez, L. Guimaraes et al., "A full-scale in situ heating test for high-level nuclear waste disposal: observations, analysis and interpretation," *Geotechnique*, vol. 59, no. 4, pp. 377–399, 2009.

[21] N. Watanabe, W. Wang, C. I. McDermott, T. Taniguchi, and O. Kolditz, "Uncertainty analysis of thermo-hydro-mechanical coupled processes in heterogeneous porous media," *Computational Mechanics*, vol. 45, no. 4, pp. 263–280, 2010.

[22] J. Rutqvist and C. F. Tsang, "Analysis of thermal-hydrologic-mechanical behavior near an emplacement drift at Yucca Mountain," *Journal of Contaminant Hydrology*, vol. 62, no. 3, pp. 637–652, 2003.

[23] M. Wang and W. Wan, "A new empirical formula for evaluating uniaxial compressive strength using the Schmidt hammer test," *International Journal of Rock Mechanics and Mining Sciences*, vol. 123, article 104094, 2019.

[24] A. Marache, J. Riss, and S. Gentier, "Experimental and modelled mechanical behaviour of a rock fracture under normal stress," *Rock Mechanics and Rock Engineering*, vol. 41, no. 6, pp. 869–892, 2008.